Design and dynamic characterization of "single-stroke" peristaltic PDMS micropumps†

Hoyin Lai and Albert Folch*

Received 14th May 2010, Accepted 16th September 2010
DOI: 10.1039/c0lc00023j

In this paper, we present a monolithic PDMS micropump that generates peristaltic flow using a single control channel that actuates a group of different-sized microvalves. An elastomeric microvalve design with a raised seat, which improves bonding reliability, is incorporated into the micropump. Pump performance is evaluated based on several design parameters—size, number, and connection of successive microvalves along with control channel pressure at various operating frequencies. Flow rates ranging 0–5.87 μL min^{-1} were observed. The micropump design demonstrated here represents a substantial reduction in the number of/real estate taken up by the control lines that are required to run a peristaltic pump, hence it should become a widespread tool for parallel fluid processing in high-throughput microfluidics.

Introduction

Drug screening is a lengthy, time-consuming process that involves a vast library of molecular candidates and a complex array of cellular targets. Advances in robotics and miniaturization have enabled high-throughput drug screening (HTDS) of molecular libraries. While efficient and precise, these robotic systems are very expensive, making it cost-prohibitive for many laboratories looking to explore novel drug candidates. At the same time, uncontrolled liquid evaporation limits the effectiveness of robotic systems in HTDS. Microfluidic systems have been developed for studying the roles of biomolecular signals,[1–5] high-throughput cell assays,[2,3,6,7] protein crystallization,[8] and polymerase chain reaction (PCR).[9,10] In these microfluidic systems, automating fluid handling across multiple microchannels is a major design consideration. To achieve cost- and space-effective automated parallel fluid processing, it is necessary to move away from expensive, bulky, off-chip equipments such as robotic fluid manipulators, and move towards scalable multiplexed arrays of on-chip microvalves and micropumps.

Various methods have been developed to control fluid flow on a microfluidic chip with microvalves (see reviews 11 and 12). These valves can be passive,[13,14] which require no external energy to operate, or active, which require external energy input from pneumatic,[8,10,15–20] thermal,[21,22] or mechanical[3,23] sources. However, passive microvalves are not amenable to complex experimental protocols that require additional fluid handling capacities, such as controlling cellular environments in microfluidic networks (μFN) spatiotemporally and processing multiple biochemical reaction steps in large-scale integrated devices. For such, a system of programmable, active microvalves is needed to control fluid movement across μFN arrays in a reproducible manner. The pneumatically actuated PDMS microvalve is the most common active valve design because of its fast response time and relatively simple fabrication procedure. A common feature in pneumatically actuated microvalves is a flexible membrane that deforms and restricts fluid flow in μFN. Peristaltic micropumps are actuated by the sequential deflection of three microvalves in series, which generates fluid displacement.[2,10,16,17,24–27] Peristalsis can also be simulated with a single control line by connecting multiple pumping elements in series by long serpentine channels so as to introduce a latency, as shown by Lee's group and others.[25,26,28,29] Whether actuated by three control lines or by a serpentine delay line, present micropump designs are very limiting because the control lines take up a large amount of on-chip real estate.

Here we present a PDMS micropump actuated by a single control line that generates peristalsis based on the principle that the various pumping elements present in the micropump are of *different sizes*. The size difference causes the microvalve membranes to deflect at different times, introducing the latency needed to generate peristalsis, regardless of connection strategies between the elements. We term this micropump a "single-stroke micropump" (SSμP). We developed a variation of the normally closed microvalve[15,17,18] that was raised 2 μm from the channel floor to simplify device bonding. The design enables three states of operations depending on the pressure applied to the control channel layer: (1) closed, when positive pressure ($P > 0$) is applied; (2) fully open, when negative pressure ($P < 0$) is applied; and (3) partially open or "leaky state", when no differential pressure ($P = 0$) is applied. We designed a SSμP that incorporates the raised-seat microvalve design in the fluidic channel; we note that the raised-seat is not essential to the functioning of the SSμP. Flow rates were measured as a function of operating frequency for various SSμP incorporating changes in one of the two design parameters—size of the pumping elements and connection strategy between the pumping elements (series or parallel).

Materials and methods

Soft lithography

Fabrication of three-layer devices with a pneumatic and fluid layer separated by a thin membrane has been described

Department of Bioengineering, University of Washington, Seattle, WA, 98195, USA

† Electronic supplementary information (ESI) available: Supplementary Fig. S1–S2 and Video S1–S3. See DOI: 10.1039/c0lc00023j

previously.[19] Briefly, silicon wafers for the fluidic layer were first spin-coated at 3000 rpm to produce a 2 μm thick layer of negative photoresist (SU-8 2002, Microchem, Newton, MA) that were exposed to collimated UV light through a transparency photomask printed at 20 000 dpi density (Fineline Imaging, Colorado Springs, CO) with the desired pattern according to manufacturer specifications. Wafers were rinsed with SU-8 developer (Microchem) before applying a second, 35 μm thick SU-8 layer to the wafers. Wafers were treated with vapor of (tridecafluoro-1,1,2,2-tetrahydrooctyl)-1-trichlorosilane (United Chemical Technologies, Bristol, PA) under vacuum before casting. The polydimethylsiloxane (PDMS) elastomer base and curing agent (10 : 1, w/w; Sylgard 184, Dow Corning, Midland, MI) were mixed and poured over the wafers, degassed, and cured overnight in an oven at 65 °C. A similar process without the 2 μm photoresist layer is used to make the control layer.

The PDMS membrane was prepared by spinning a mixture of hexane and uncured PDMS (1 : 3, w/w) at 7000 rpm on a clean, fluorosilane-treated silicon wafer for 30 s and cured on a hotplate for 90 minutes at 85 °C.[30] The resulting membrane had a thickness of 12 μm.

Bonding

The three PDMS layers were assembled by plasma bonding as depicted schematically in Fig. 1b using the protocol described previously.[19] Both sides of the PDMS layers were cleared of surface debris with Scotch tape. The control layer and thin membrane were exposed to oxygen plasma (Plasma Preen II, Plasmatic Systems Inc., North Brunswick, NJ), pressed together to bond the layers and subsequently placed on a hotplate for 30 min at 85 °C to complete the bonding process. After 30 min, cuts were made around the edges of the pneumatic control layer and the mold was peeled from the wafer.

Inlet ports were punched into the fluidic channel layer using a 1.0 mm micropuncher (Harris Uni-Core™, purchased from Ted Pella, Redding, CA). An 18 gauge blunt end needle with 90° bends (Small Parts) was inserted into the control layer inlets to provide vacuum access during device assembly. Membranes covering the inlets were removed with tweezers to allow fluid access into the control channels after plasma treatment. The membrane shielded the control channel from the oxygen plasma. The layers were brought into contact under a stereomicroscope and were then connected to a house vacuum source with a bleed line to separate the membrane from the valve seat. The assembled devices were placed on the hotplate at 85 °C with the vacuum setup for 5 minutes and tested with an air-filled syringe. The devices were tested within 30 minutes of assembly. We deliberately chose to test the devices immediately after assembly as a method of standardizing the experimental protocol. As PDMS ages over extended period of time, the pumping performance must be re-calibrated for long-term storage, which was beyond the scope of this study.

Flow rate measurements

A solenoid valve system controlled by a custom LabView program is used to operate the micropump. The solenoid valve alternated between positive pressure (9 psi) and negative pressure

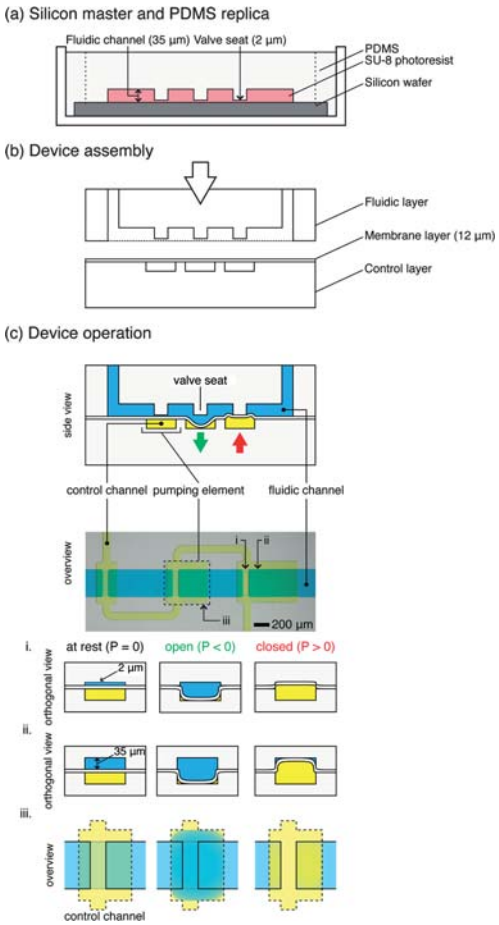

Fig. 1 *Overview of "single-stroke" micropump (SSμP) fabrication and operation.* (a) Fabrication of the PDMS micropump by soft lithography. Silicon masters (*not shown*) of the fluidic layer and control layer are fabricated by photolithography using SU-8 negative photoresist; replica layers are made by pouring PDMS polymer (10 : 1 w/w, prepolymer : crosslinker) onto silanized masters. (b) Assembly of fluidic layer, control layer, and PDMS membrane by O_2-plasma bonding. Thin PDMS membrane is spun onto clean, silanized silicon wafers, cured, and subsequently bonded to the control layer after O_2-plasma exposure; access ports are opened in the fluidic layer and bonded under vacuum to the control layer and thin membrane. (c) *Top half:* Schematic representation and stereomicrograph of a SSμP; *bottom half*: operation schematic of a microvalve. Orthogonal cross-section of the microvalve at the valve seat (i) and above the pumping element (ii) is depicted along with the overview of the microvalve (iii). At rest, the valve is partially open due to the gap between the valve seat and thin membrane in the fluidic channel; in this "leaky state", the microvalve functions as a flow resistor that restricts large particles and reduces fluid flow. When positive pressure is applied, the thin membrane deflects upward, pressing against the raised valve seat, effectively closing the channel; however, only the raised valve seat is closed completely while the region with regular channel height is not, due to the rectangular geometry of the channel. The volume displaced by the deflecting thin membrane into the 35 μm tall region of the channel provides the bulk of fluid flow in pumping operations. When vacuum is applied, the thin membrane deflects downward, revealing a large opening for fluid passage beneath the valve seat; the vacuum stroke speeds up air evacuation from the pressurized state and also enables greater fluid filling.

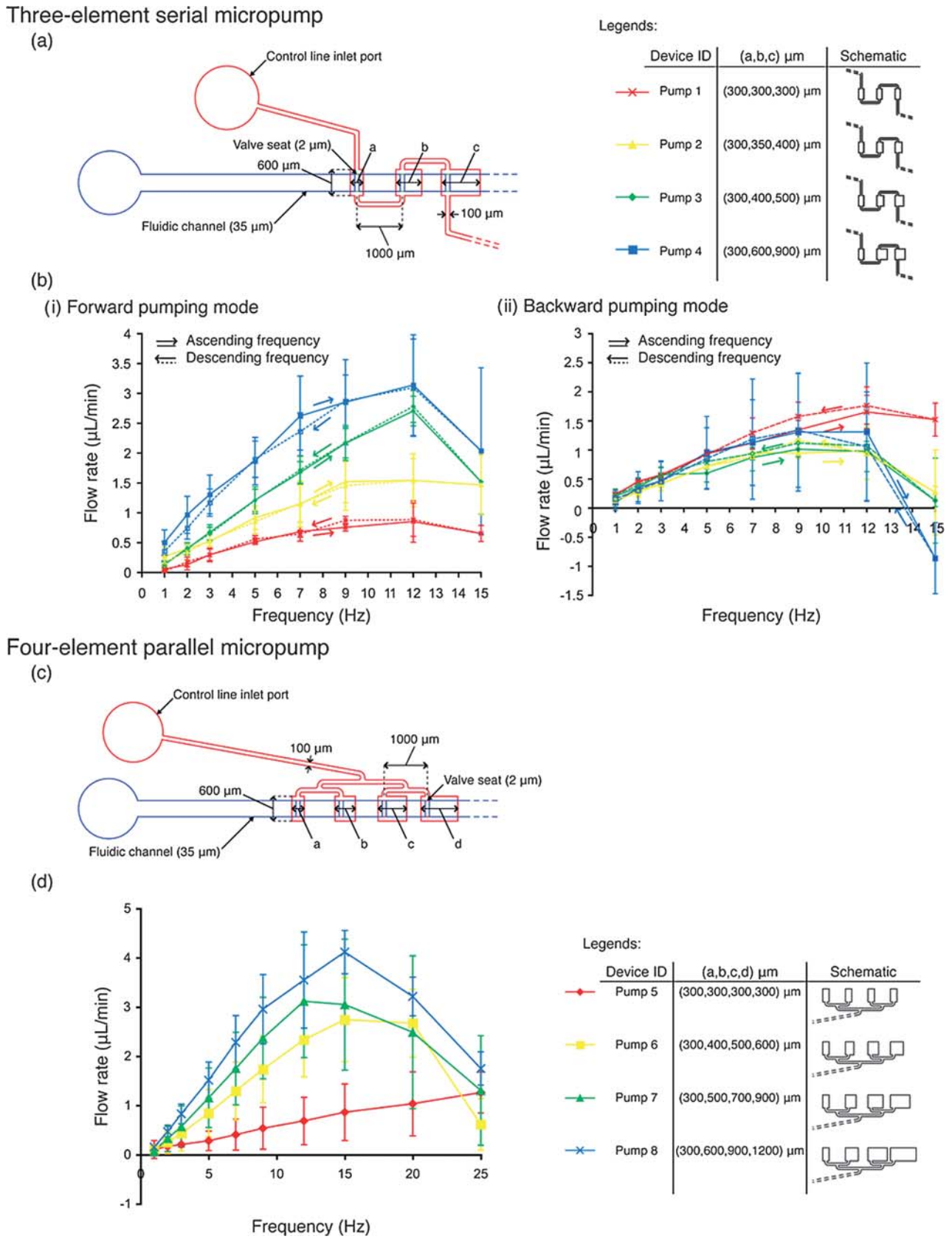

Fig. 2 *Flow rate characterization for eight designs of the single-stroke micropump (SSμP).* Three-element serial SSμP (a) design schematic and (b) flow rate measurement in (i) forward and (ii) backward pumping mode. Measurements were taken in the sequence of ascending frequency (solid lines) initially followed by a descending sequence (dotted lines) to test membrane hysteresis. Four-element parallel SSμP (c) design schematic and (d) flow rate measurement.

(−10 psi) at a frequency specified by the computer program. The channels were filled, or primed, with diH_2O until the fluid front inside the silicone tubing comes into view of the stereomicroscope. The priming fluid was pressurized with an air-filled syringe for 2 minutes to drive out air bubbles trapped in the fluidic channel. (The bubbles disappeared into the PDMS bulk.) Complete wetting of the fluidic channel reduced the potential for bubble formation during pump operations. Still images were acquired at one minute intervals on a digital SLR camera (Canon EOS 5D Mk II, Canon USA, Lake Success, NY) controlled by a remote capture program on the computer (EOS Utility, Canon) while the pump controller program is running. Acquired images were imported into ImageJ (National Institute of Health, Bethesda, MD) and the position of the fluid front was measured. Volumetric flow rate was calculated as a cylindrical volume as a function of the distance traveled by the fluid front in one minute.

Results and discussion

Device overview and operation

A schematic of the micropump design and operation is shown in Fig. 1c. Despite the raised valve seat, the microvalves in our design operate the same way as the normally closed microvalve design.[15,17,18] Applying positive pressure in the control channel seals the fluidic channel and stops fluid flow; while applying negative pressure opens the fluidic channel and restores fluid flow in full, as shown in Fig. 1c. Irreversible bond between the valve seat and the deflectable membrane during plasma bonding of other devices presents a problem for assembly. Several methods, such as using conformal bonding property of PDMS,[17,18] protecting the valve seat with micropatterned metal pads,[31] and partial curing of PDMS layers,[32] have been proposed to solve the problem, though each with their own trade-offs. Implementation of the raised valve seat in the valve design presented in this paper enables straightforward plasma bonding of the device. At the same time, the raised valve seat also causes the valve to leak when the membrane is not pressurized in operation. When positive pressure is applied, the microvalve shuts off fluid flow completely and no fluorescent leakage is observed (see Figure S1†). In principle, the leaky state could be used as a flow resistor.[33]

Micropump design principle

The micropump's design principle is that the membranes of the microvalves (or, more generally speaking, "pumping elements", since the membrane may not be on a seat) act as a mechanical resonator, each with a characteristic response time defined by their inertial mass. Therefore, all the pumping elements can be connected to the same pneumatic line (either in series or in parallel, as we discuss below), since they effectively act as temporal filters: even though the group of membranes receive the driving pressure pulse at (almost) the same time, the smallest responds the fastest (it has the least inertia) and the largest responds the slowest. Since the micropump is designed to generate peristalsis from a single pressure stroke without the introduction of delays, as in Lee's design,[25,26,29] we term this design a "single-stroke micropump" (SSμP). The term "SSμP" also applies to other pumps that are driven with a single pressure inlet; we use the term only to simplify its designation within this manuscript.

We note that our pumps' operating frequency ranges around 12–15 Hz (on the same order of magnitude as most PDMS pumps reported in the literature), so given the velocity of sound in dry air (~343 m s^{-1} at 20 °C), a pressure pulse used to actuate the pumps would take ~14.6 μs to cover the ~5 mm (assuming rigid microchannels) that the device spans (from smallest membrane to largest membrane). This amount of time is insignificant compared to the response time of the membranes (60–80 ms = (12–15 Hz)$^{-1}$). In order to design delay lines that can start affecting the membranes (introducing delays in the order of ~10 ms, neglecting the microchannel's aerodynamic passive resistance to air), they would have to be 343 m s^{-1} × 10^{-3} s = 3.43 m (!) long—clearly impractical. Lee's designs have shown that, since PDMS is elastic and the volume V of the channels expands with applied pressure P, they can be considered to have a "capacitance", $C = dV/dP$ (and their aerodynamic resistance is actually not negligible), which lowers the response time of the circuit, so the delay lines can be on the order of ~1 cm.[25,26,28,29] Still, this approach imposes a high tax on the real estate of the device. Our design principle was conceived to eliminate all delay lines.

Size of pumping elements

The size of the pumping elements is an important design parameter, since it determines the dynamic response of the membranes, such as the peak operating frequency, as well as the volume displaced per stroke. In general, larger pumping elements displace larger fluid volume with each stroke and thus increase maximum flow rate. At the same time, the large elements require longer time to fill and evacuate, thus limiting their peak operating frequency.

We started our study with a simple, three-element SSμP design with the elements connected in series (Fig. 2a). All three-element SSμP have two pneumatic inputs, one on each end of the control channel. The length of each element ranges from 300 μm to 900 μm with a width of 600 μm. The channel connecting successive elements is 100 μm wide and 1000 μm long. The micropump design occupies an area of roughly 3000 μm by 800 μm, which is smaller than the 5500 μm by 2000 μm serpentine micropump reported by Lee and coworkers[26] (the optimal design for Lee's pump would also include two 15 000 μm long connecting channels, which are required to provide the time-delay but pose clear compactness problems). In our SSμPs, microvalves are located in the fluidic channel and placed asymmetrically with respect to each element—100 μm from the upstream edge. Incorporation of the microvalves prevents backflow during operation of the pump while the asymmetric location of the valve seats (a feature that is not essential for pump operation) increases volume displacement downstream during the pressure stroke. Fig. 2b plots the relationship between flow rate and operating frequency for four different designs of three-element SSμPs. Higher flow rate is observed with larger micropumps and higher operating frequency, peaking at ~12 Hz. The highest flow rate achieved in this group of three-element SSμPs is 3.14 ± 0.84 μL min^{-1}, corresponding to the largest design—Pump 4 (×).

We tested the micropumps in reverse order to determine the effect of element order on flow rate. For this experiment, the downstream inlet closest to the largest pumping element is used; we define this mode as "backward pumping", as opposed to the normal connection using the source inlet, which we define as "forward pumping". As shown in Fig. 2b–ii, the flow rates in the backward pumping mode are lower than the flow rates in the forward pumping mode (Fig. 2b–i). The backward pumping flow rate curves for all four SSμP designs are within the standard error of each other and are similar to the forward flow rate of Pump 1, which has all identical pumping elements. The asymmetry in measured flow rate for Pumps 2–4 in forward *vs.* backward pumping mode reinforces our notion that the asymmetric valve positions contribute to increased forward flow. Hysteresis measurements (dotted lines) are in line with our findings from the forward pumping mode results.

We believe that the reason why the forward mode is more effective than the backward mode is the location of the valve seat. As the valve closes, the first place to be shut off is the seat. As a result, the valves use the area to the right of the seats in forward mode and to the left of the seats in backward mode. Hence, in backward mode, the effective pump volume is much smaller than in forward mode. We have found that the pumps display a proportionality behavior: their right-to-left size ratio (defined as the sum of the volumes to the right of the seat divided by the sum of the volumes to the left of the seat) is proportional to their forward-to-backward average pumping ratio (defined as the ratio of flow rates achieved in forward *vs.* backward mode, averaged for all frequency values between 1 and 12 Hz) as shown in Fig. S2†. (Past 12 Hz, the pumps undergo incomplete cycles and occasionally (Pump 4) display odd behaviors such as pumping backwards.)

Four-element binary tree pump

As demonstrated by Lee and co-workers, serially connected chambers will introduce delays because the membranes themselves behave like RC circuits.[25,26,29] To eliminate delays altogether, we devised a four-element, parallel-connection micropump design where pressure strokes arrive at all pumping elements simultaneously. Fig. 2c shows the design and dimensions of a 4-element SSμP. The pumping elements are connected in parallel by 100 μm wide pneumatic channels that branch off in a binary fashion and are separated at a distance of 1000 μm. Four size increment values ($\Delta = b - a = 0$, 100, 200, 300 μm) are used to design the parallel four-element micropumps with pumping elements ranging from 300 μm to 1200 μm long and 600 μm wide. Fig. 2d shows flow rate curves for four micropump designs. As expected, pump designs with larger elements generated higher flow rate than pumps with smaller elements. Wider range of operating frequency and a higher peak frequency, at about 15 Hz, are observed. The maximum flow rates for the four designs (Pumps 5 to 8) are 1.26 ± 0.42, 2.74 ± 0.86, 3.12 ± 1.15, and 4.11 ± 0.44 μL min^{-1}, with operating frequency peaking at 25, 15, 12, and 15 Hz, respectively.

Interestingly, despite the simultaneous actuation of all four (equal-size) elements in Pump 5, forward pumping flow was still observed. We attribute the forward flow to alignment errors that resulted in asymmetrical position of the microvalve over the elements. This misalignment results in slightly higher displacement volume downstream. While simultaneous actuation of the elements restricts forward flow in the first three elements, the fourth element can still displace fluid downstream since there are no other valves to restrict flow. However, more experiments, possibly with a high-frame rate video camera, are needed to determine the exact cause of the forward flow for the parallel 4-element SSμP.

Sequential actuation of different-sized pumping elements

To observe the actuation sequence of the different SSμPs, we recorded videos (obtained at 30 frames per second with an SLR camera) of the running micropumps and extracted individual frames using video-editing software (Adobe Premiere Elements 3.0, Adobe Systems Inc., San Jose, CA) for analysis. (Videos are available in the ESI† as Videos S1 and S2.) Frame sequences for one pump cycle of the three-element serial and four-element parallel SSμPs are shown in Fig. 3. We used Pump 3 for the three-element SSμP and a modified Pump 8 with only one microvalve for the four-element SSμP. A yellow dye is used to visualize the control channel and as the working fluid for the micropump, whereas the control channel was filled with air for flow measurements. The size of the pumping element affects its response time, with larger elements deflecting more slowly compared to the smaller elements. The lag in larger elements was more dramatic in the serial SSμP (Fig. 3a) than in the parallel SSμP (Fig. 3b). In addition, the four-element SSμP displayed second-order membrane buckling in the third and fourth element during the pressure stroke shown at the 0:03.200 time point of Fig. 3b. We attribute this buckling behavior to residual pressure in the fluidic channel that prevented the closure of the microvalve. Using air as the driving fluid for the control channel

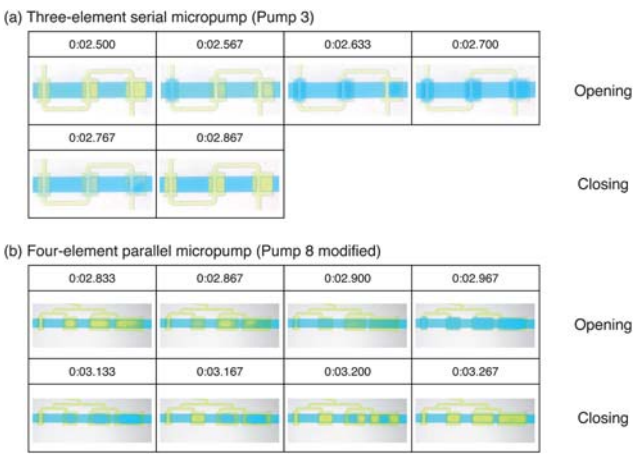

Fig. 3 *Sequential activation of different-sized elements in serial and parallel single-stroke micropumps (SSμPs).* Frame-by-frame sequence of (a) three-element serial (Pump 3) and (b) four-element parallel (Pump 8 modified) SSμPs. Frames are obtained from video showing the pumping sequence of each pump (video is available in the ESI†) recorded at 30 fps and high definition with an SLR camera. Time of each frame is presented as shown in the actual video footage with the time format minute:-second.millisecond. The four element parallel pump used in the video is modified from the original design by removing the last three microvalves from the fluidic channel.

should reduce the effect of residual pressure in the fluidic channel.

Micropump performance at different control channel pressures

Previous studies of open-at-rest micropumps[16,25] have shown that flow rate changes with control channel pressures across the operating frequency spectrum with higher flow rates associated with greater control channel pressures, probably due to deformation of the control channel into the fluid-carrying channel. Unlike the micropumps reported by others,[16,25] our micropump designs show no changes in flow rate with different control channel pressures at low frequency. The serial 5-element micropump used in this experiment is shown in Fig. 4a. The lengths of the elements range from 300 μm to 900 μm (Δ = 150 μm per successive element) and the width is 600 μm. The pumping elements are connected in series by pneumatic channels of length 1000 μm and width of 100 μm. Fig. 4b depicts a flow characterization curve of the serial 5-element micropump with control channel pressures of 6, 9, and 12 psi. However, as the operating frequency increases (past ~10 Hz), the performance of the micropumps begins to diverge (note that the pump even pumps backward above 14 Hz), shifting the optimal operating frequency to the right with increasing pressure. The peak operating frequencies for the 5-element micropumps are 9 Hz, 12 Hz, and 15 Hz for control channel pressure of 6 psi, 9 psi, and 12 psi, producing maximum flow rates of 3.13 ± 1.57, 4.63 ± 1.77, and 5.87 ± 2.02 μL min^{-1}, respectively.

We attribute this pressure-independence at low frequency to the incorporation of microvalve seats and higher pressure gradient in our design. The microvalves are capable of fast switching between open and closed state because of its shallow position in the midpoint between the fully open and fully closed states. In the normally open microvalve design (*e.g.* Quake's PDMS valves[16]), the membrane must deflect the entire height of the fluidic channel before the channel becomes completely sealed. Fluid displacement is divided equally between upstream and downstream until the first microvalve closes, after which flow is driven only in the downstream direction. With slower-responding microvalves, the subsequent elements begin to deflect before the first microvalve is fully closed; this results in higher share of the fluid volume being displaced upstream, thus reducing pump efficiency. In our design, the microvalve switches to the closed state before the membrane completes the pumping stroke, thereby improving downstream flow output.

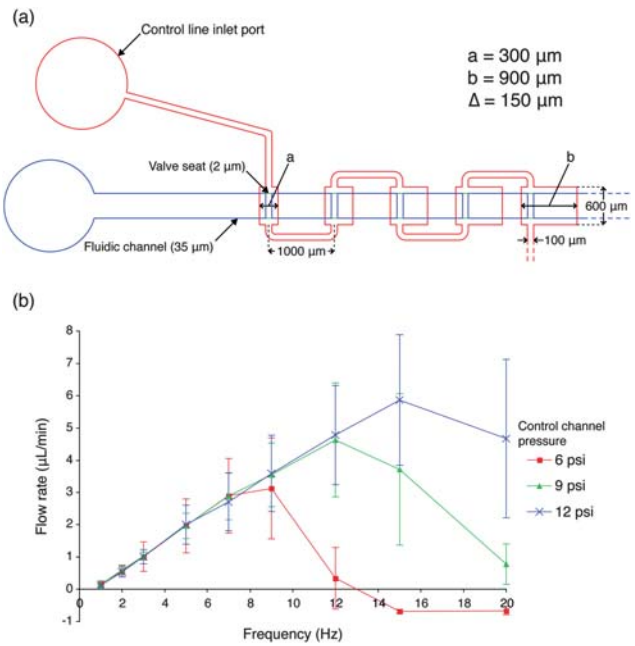

Fig. 4 *Effect of control channel pressure on flow rate* versus *operating frequency*. (a) Design of serial, 5-element SSμP used in the experiment; the smallest elements (*a*) and the largest elements (*b*) have lengths of 300 and 900 μm, respectively, with increment lengths (Δ) of 150 μm. (b) Flow rate measurement curve at selected operating frequencies for the 5-element micropump design with control channel pneumatic pressures of 6, 9, and 12 psi.

We included a vacuum stroke in the pumping sequence that accelerates evacuation of the control line, whereas most PDMS microvalves and micropumps[16–18,24–26] use pressure to deflect the membrane and rely on the elasticity of the PDMS to revert the membrane to its undeflected state. In high-frequency operation, elastic membrane recovery is limited by the characteristic response time of the membrane itself, thus producing incomplete pumping strokes. In our control scheme, we can maintain a greater pressure gradient (from +12 to −10 psi, a total of 22 psi differential, compared to a differential of +15 to 0 psi in ref. 16) using a combination of pressure and vacuum strokes. The greater pressure gradient enhances working fluid evacuation in the membrane recovery state, resulting in a greater number of complete open-close cycles. At the same time, the vacuum stroke generates additional pumping volume from fluids filling the cavity created by deflection of the membrane into the control channel. This results in the displacement of two cavity volumes of fluid per stroke—half from membrane recovery from the open to closed state and another half from membrane deflection into the fluidic channel roof. However, at low input pneumatic pressure, the switch from negative to positive pressure is very inefficient at high frequency because the time between vacuum strokes is insufficient to inflate the pumping element, thereby essentially creating an always-open state for the valve. Conversely, having too high pneumatic pressure will result in the insufficient evacuation of the pumping element, resulting in an always-closed valve.

The pressure-independence behavior at low operating frequency exhibited by our proposed micropump design is amenable to very large-scale integration. Multiple pumps can be operated in parallel using a single control channel with minimal effect on individual pump performance due to a drop in input pressure from the extra branches. Additionally, the pump design can be incorporated into devices where pneumatic inputs are limited, though the need for a vacuum source makes the deployment difficult for point-of-care applications. In future studies, we will further optimize the design parameters and incorporate the proposed microvalve and micropump design into large-scale integrated platforms for microfluidic cell culture devices.

Conclusion

A compact peristaltic PDMS micropump, termed the "single-stroke micropump" (SSμP), that requires only one control

channel and is based on three or more pumping elements of increasing size and at least one valve seat, has been tested and characterized. Microvalves based on the normally closed design with asymmetric valve seats raised 2 μm above the fluidic channel floor were incorporated into the SSμP; other combinations of positions of valve seats are possible (only the first seat, on the smallest valve, is strictly necessary to trigger flow). The raised valve seat facilitated plasma bonding of the devices. The maximum flow rate of 5.87 ± 2.02 μL min^{-1} was observed at 15 Hz for a 5-element serial connection micropump operating with 12 psi of control channel pressure. We have observed that flow generated by the micropumps is independent of control channel pressure at low frequency. Additionally, reversible pumping was demonstrated with the serial connection SSμP. The microvalve and micropump design presented here can be implemented into a wide range of microfluidic devices to manipulate fluid flow. Furthermore, the SSμP operating principle can be extended to operate multiple micropumps for highly parallel fluidic processing and for high-throughput screening (a proof-of-concept system with three pumps running in parallel is shown in ESI, see Video S3†).

References

1 A. Tourovskaia, X. Figueroa-Masot and A. Folch, *Lab Chip*, 2005, **5**, 14–19.
2 R. Gomez-Sjoberg, A. A. Leyrat, D. M. Pirone, C. S. Chen and S. R. Quake, *Anal. Chem.*, 2007, **79**, 8557–8563.
3 N. Futai, W. Gu, J. W. Song and S. Takayama, *Lab Chip*, 2006, **6**, 149–154.
4 A. Tourovskaia, N. Li and A. Folch, *Biophys. J.*, 2008, **95**, 3009–3016.
5 C. W. Frevert, G. Boggy, T. M. Keenan and A. Folch, *Lab Chip*, 2006, **6**, 849–856.
6 T. Thorsen, S. J. Maerkl and S. R. Quake, *Science*, 2002, **298**, 580–584.
7 K. R. King, S. H. Wang, D. Irimia, A. Jayaraman, M. Toner and M. L. Yarmush, *Lab Chip*, 2007, **7**, 77–85.
8 C. L. Hansen, M. O. Sommer and S. R. Quake, *Proc. Natl. Acad. Sci. U. S. A.*, 2004, **101**, 14431–14436.
9 J. Khandurina, T. E. McKnight, S. C. Jacobson, L. C. Waters, R. S. Foote and J. M. Ramsey, *Anal. Chem.*, 2000, **72**, 2995–3000.
10 J. Liu, C. Hansen and S. R. Quake, *Anal. Chem.*, 2003, **75**, 4718–4723.
11 C. Zhang, D. Xing and Y. Li, *Biotechnol. Adv.*, 2007, **25**, 483–514.
12 J. Melin and S. R. Quake, *Annu. Rev. Biophys. Biomol. Struct.*, 2007, **36**, 213–231.
13 D. J. Beebe, J. S. Moore, J. M. Bauer, Q. Yu, R. H. Liu, C. Devadoss and B. H. Jo, *Nature*, 2000, **404**, 588–590.
14 C. W. Liu, J. Y. Park, Y. G. Xu and S. Lee, *J. Micromech. Microeng.*, 2007, **17**, 1985–1991.
15 K. Hosokawa and R. Maeda, *J. Micromech. Microeng.*, 2000, **10**, 415–420.
16 M. A. Unger, H. P. Chou, T. Thorsen, A. Scherer and S. R. Quake, *Science*, 2000, **288**, 113–116.
17 W. H. Grover, A. M. Skelley, C. N. Liu, E. T. Lagally and R. A. Mathies, *Sens. Actuators, B*, 2003, **89**, 315–323.
18 N. Li, C. H. Hsu and A. Folch, *Electrophoresis*, 2005, **26**, 3758–3764.
19 G. A. Cooksey, C. G. Sip and A. Folch, *Lab Chip*, 2009, **9**, 417–426.
20 D. Irimia and M. Toner, *Lab Chip*, 2006, **6**, 345–352.
21 R. H. Liu, J. Bonanno, J. N. Yang, R. Lenigk and P. Grodzinski, *Sens. Actuators, B*, 2004, **98**, 328–336.
22 W. van der Wijngaart, D. Chugh, E. Man, J. Melin and G. Stemme, *J. Microelectromech. Syst.*, 2007, **16**, 765–774.
23 D. B. Weibel, M. Kruithof, S. Potenta, S. K. Sia, A. Lee and G. M. Whitesides, *Anal. Chem.*, 2005, **77**, 4726–4733.
24 N. Sundararajan, D. S. Kim and A. A. Berlin, *Lab Chip*, 2005, **5**, 350–354.
25 C. H. Wang and G. B. Lee, *J. Micromech. Microeng.*, 2006, **16**, 341–348.
26 S. B. Huang, M. H. Wu, Z. F. Cui, Z. Cui and G. B. Lee, *J. Micromech. Microeng.*, 2008, **18**, 045008.
27 O. C. Jeong and S. Konishi, *J. Micromech. Microeng.*, 2008, **18**, 085017.
28 J. B. Shao, L. Wu, J. Z. Wu, Y. H. Zheng, H. Zhao, Q. H. Jin and J. L. Zhao, *Lab Chip*, 2009, **9**, 3118–3125.
29 C. W. Huang and G. B. Lee, *J. Micromech. Microeng.*, 2007, **17**, 1266–1274.
30 J. M. Hoffman, J. Shao, C. H. Hsu and A. Folch, *Adv. Mater.*, 2004, **16**, 2201–2206.
31 D. Irimia and M. Toner, *Lab Chip*, 2006, **6**, 345–352.
32 J. S. Go and S. Shoji, *Sens. Actuators, A*, 2004, **114**, 438–444.
33 E. W. Lam, G. A. Cooksey, B. A. Finlayson and A. Folch, *Appl. Phys. Lett.*, 2006, **89**, 164105.

